

# Schwinger boson mean field theory: numerics for the energy landscape and gauge excitations in two-dimensional antiferromagnets

G. Misguich<sup>1</sup>

<sup>1</sup> *Institut de Physique Théorique, CEA, IPhT, CNRS, URA 2306, F-91191 Gif-sur-Yvette, France.*

We perform some systematic numerical search for Schwinger boson mean field states on the square, triangular and kagome clusters. We look for possible inhomogeneous ground states as well as low-energy excited saddle points. The spectrum of the Hessian is also computed for each solution. On the square lattice we find gapless  $U(1)$  gauge modes in the non-magnetic phase. In the  $\mathbb{Z}_2$  liquid phase of the triangular lattice we identify the topological degeneracy as well as vison states. The energy landscape on kagome lattices shows tiny energy scales and we discuss its relation to classical planar states.

## I. INTRODUCTION

Quantum antiferromagnets can display complex many body phenomena, with rich phase diagrams, exotic states of matter with emerging degrees of freedom.<sup>1</sup> Indeed, minimizing a rather simple looking interaction like the Heisenberg one,  $\vec{S}_i \cdot \vec{S}_j$ , can lead to a vast variety of states of matter, depending on the size  $\vec{S}_i^2 = S(S+1)$  of the spins, the space dimension, geometry of the lattice, or relative strengths of possible competing interactions (frustration, etc.). In fact, after many years of theoretical investigations, the nature of the ground state of the spin- $\frac{1}{2}$  Heisenberg model remains controversial on several two and three dimensional lattices (like the kagome and pyrochlore). Some of the most interesting states that can be stabilized at  $T = 0$  are called *spin liquids* and have no direct classical analogs. These systems remain rotationally invariant down to zero temperature. There is a whole zoo of possible spin liquids, and the most exotic one have low energy excitations which carry a half-odd-integer spin (unlike conventional spin waves).

There are rather few theoretical tools that are able to describe the limit of strong quantum fluctuations (small  $S$ ) for these systems, and spin liquid phases in particular. Among them, the so-called large- $N$  techniques, introduced by Affleck for spin chains,<sup>2</sup> play a central role. By generalizing the symmetry group of global spin rotations from  $SU(2)$  to some larger group like  $SU(N)$  or  $Sp(2N)$ ,<sup>3</sup> the model can be solved in the limit  $N = \infty$ . Of course, the physics for  $N = 2$  needs not be simply related to that at  $N = \infty$ . However, the success of these approaches is in part due to the fact that a number of interesting states that can be realized for  $SU(2)$  models, also exist in the  $N = \infty$  phase diagrams. In particular, the  $N = \infty$  models are not restricted to have magnetically ordered ground state, and can have resonating valence-bond spin liquids ground states with fractionalized excitations and emerging gauge degrees of freedom. Furthermore, the effect of finite- $N$  corrections (both perturbative<sup>4,5</sup> and non-perturbative ones<sup>6</sup>) can be addressed.

In this work we consider a particular large- $N$  limit, the so-called Schwinger boson mean field theory (SBMFT).<sup>3,7</sup> It has been applied to many two-

dimensional systems, such as the  $J_1 - J_2$  square,<sup>8</sup> triangular,<sup>9-11</sup> honeycomb<sup>12,13</sup>, kagome,<sup>9,14-16</sup>, kagome with further neighbor interactions,<sup>16,17</sup> or Shastry-Sutherland<sup>18,19</sup> or  $\text{CaV}_4\text{O}_9$ ,<sup>20</sup> lattices. This limit can in particular stabilize magnetically ordered (Néel) states as well as  $\mathbb{Z}_2$  spin liquids with gapped spinons.<sup>9</sup>

The model contains  $N$  flavors of spin- $\frac{1}{2}$  bosons (spinons) and the parameter which plays the role of the spin value  $2S$  is the number  $\kappa$  of bosons per site (and per flavor). After performing a Hubbard-Stratonovich decoupling of the boson-boson interaction, the different boson flavors are coupled to a single complex field  $A_{ij}$  on each bond  $ij$  of the lattice. The formal (Gaussian) integration of the spinons gives an effective action  $S_{\text{eff},N}[A]$  for the bond field. But the dependence in  $N$  is simple since this action is that of the single-flavor problem multiplied by a factor  $N$ :  $S_{\text{eff},N}[A] = NS_{\text{eff},1}[A]$ . When  $N$  is large it is therefore natural to perform a saddle point expansion. At the saddle point the bond-field fluctuations are frozen, and the effective Hamiltonian is simply quadratic in the spinon operators. So the action can be computed with the help of a standard Bogoliubov transformation. Finding a the large- $N$  ground state thus amounts to solving a classical minimization problem.

Previous SBMFT studies have mostly been focused on the ground state properties at  $N = \infty$ . However, as a first step to understand the effects of finite- $N$  corrections, it is interesting to have access to the low-energy energy landscape of saddle points. Although the system is locked into the lowest one when  $N = \infty$ , the (large but) finite- $N$  physics must include some fluctuations between different low-energy saddle points, as well as some (perturbative in  $1/N$ ) fluctuations in the vicinity of each of these saddle point. Our goal here is to provide a quantitative description of the/some excited saddle points.

In order to reduce the number of variables, it is almost always assumed that the lowest-energy state preserves most (or at least some) of the lattice symmetries (see Ref.<sup>21</sup> for a notable exception). In practice most numerical studied have so far been restricted to a solutions with a unit cell including a few sites only. This is a reasonable assumption for the ground state, and we confirm validity in several cases. However, since we are interested here in excited saddle points, we need to be able to com-

pute some *spatially inhomogeneous* states as well. We will however limit ourselves to time-independent solutions.

In this work perform some extensive numerical minimization to look for the ground state and low-energy excited states on clusters containing up to 144 sites. We compare the results we obtain on three different lattices (square, triangular and kagome), and for different values of the boson density (“spin”)  $\kappa$ .

## II. SCHWINGER BOSON MEAN FIELD THEORY

To keep this article self-contained, this section presents the basic ideas and notations of the SBMFT (see also Refs.<sup>22,23</sup>).

“up” and “down” bosons operators ( $\sigma \in \{\uparrow, \downarrow\}$ ), carrying a  $S = 1/2$ , are introduced at each lattice site:  $b_{i\sigma}^\dagger$  and  $b_{i\sigma}$ . The spin operators can then be written:

$$S_i^+ = b_{i\uparrow}^\dagger b_{i\downarrow} \quad (1)$$

$$S_i^- = b_{i\downarrow}^\dagger b_{i\uparrow} \quad (2)$$

$$S_i^z = b_{i\uparrow}^\dagger b_{i\uparrow} - b_{i\downarrow}^\dagger b_{i\downarrow} \quad (3)$$

These relations imply that the commutation relations  $[S_i^\alpha, S_i^\beta] = i\epsilon^{\alpha\beta\delta} S_i^\delta$  are automatically verified. The total spin reads  $\vec{S}_i^2 = \frac{n_i}{2} \left( \frac{n_i}{2} + 1 \right)$ , where  $n_i = b_{i\uparrow}^\dagger b_{i\uparrow} + b_{i\downarrow}^\dagger b_{i\downarrow}$  is the total number of bosons at site  $i$ . To fix the “length” of the spins, the following constraint must therefore be imposed on physical states:

$$\forall i, \quad \sum_{\sigma} b_{i\sigma}^\dagger b_{i\sigma} = \kappa = 2S \quad (4)$$

The Heisenberg exchange Hamiltonian is biquadratic in the  $b$  operators and reads

$$H = \sum_{\langle ij \rangle} J_{ij} \mathbf{S}_i \cdot \mathbf{S}_j \quad (5)$$

$$= \frac{1}{4} \sum_{\langle ij \rangle} J_{ij} \left( b_{i\sigma}^\dagger \vec{\sigma}_{\sigma, \sigma'} b_{i\sigma'} \right) \cdot \left( b_{j\tau}^\dagger \vec{\sigma}_{\tau, \tau'} b_{j\tau'} \right), \quad (6)$$

where  $\vec{\sigma}$  is the vector whose components are the Pauli matrices, and each lattice bond  $ij$  is taken only once. It is convenient to re write  $H$  using rotationally invariant bond operators:

$$H = \sum_{\langle ij \rangle} J_{ij} \left( : \hat{B}_{ij}^\dagger \hat{B}_{ij} : - \hat{A}_{ij}^\dagger \hat{A}_{ij} \right), \quad (7)$$

where  $: - :$  represents normal ordering and the bond operators  $\hat{A}_{ij}$  and  $\hat{B}_{ij}$  are

$$\hat{A}_{ij} = \frac{1}{2} (b_{i\uparrow} b_{j\downarrow} - b_{i\downarrow} b_{j\uparrow}) \quad (8)$$

$$\hat{B}_{ij} = \frac{1}{2} (b_{i\uparrow}^\dagger b_{j\uparrow} + b_{i\downarrow}^\dagger b_{j\downarrow}). \quad (9)$$

$\hat{A}_{ij}^\dagger$  creates a spin singlet on the (oriented) bond  $ij$  whereas  $\hat{B}_{ij}^\dagger$  creates a triplet. Due to the constraints, these operators are linked by the relation

$$: \hat{B}_{ij}^\dagger \hat{B}_{ij} : + \hat{A}_{ij}^\dagger \hat{A}_{ij} = S^2. \quad (10)$$

and it is therefore possible to express the Hamiltonian using  $\hat{A}$  only:

$$H = \sum_{\langle ij \rangle} J_{ij} \left( S^2 - 2\hat{A}_{ij}^\dagger \hat{A}_{ij} \right). \quad (11)$$

The SB mean field approximation – which can be formally justified in a large- $N$  limit of the model – consists in decoupling the quartic terms and to add some chemical potentials  $\lambda_i$  to tune the *average* number of boson at each site (instead of Eq. 4). The resulting mean field Hamiltonian is

$$H_{\text{MF}} = \sum_{\langle ij \rangle} J_{ij} \left( S^2 - 2\bar{A}_{ij} \hat{A}_{ij} - 2A_{ij} \hat{A}_{ij}^\dagger + 2|A_{ij}^2| \right) - \sum_i \lambda_i \left( b_{i\sigma}^\dagger b_{i\sigma} - 2S \right) \quad (12)$$

where  $\bar{x}$  is the conjugate of  $x$ ,  $A_{ij}$  are complex link variables with property  $A_{ij} = -A_{ji}$ . It is also possible to write a mean field theory keep simultaneously both operators  $\hat{A}$  and  $\hat{B}$  on each bond.<sup>24,25</sup> This will however not be considered here.<sup>26</sup>

It is convenient to write  $H_{\text{MF}}$  by grouping the creation and annihilation operators in a vector  $\hat{\phi} = (b_{1\uparrow}, \dots, b_{N\uparrow}, b_{1\downarrow}, \dots, b_{N\downarrow})^t$ :

$$H_{\text{MF}} = (\hat{\phi})^\dagger M \hat{\phi} + \text{cst.} \quad (13)$$

where the  $M$  is a  $2N \times 2N$  matrix :

$$M = \begin{bmatrix} -\lambda_i & J_{ij} A_{ij} \\ -J_{ij} \bar{A}_{ij} & -\lambda_i \end{bmatrix}. \quad (14)$$

For simplicity, we restrict the discussion to finite systems where  $H_{\text{MF}}$  has a gapped spectrum (possibly vanishing in the thermodynamic limit). The ground state exists and its spectrum is gapped if and only if the the matrix  $M$  is positive definite.<sup>27</sup> We define a diagonal  $2N \times 2N$  matrix  $\sigma$ :  $\sigma = \begin{bmatrix} -1 & 0 \\ 0 & 1 \end{bmatrix}$  and, with the gap condition,  $\sigma M$  is diagonalizable (although not Hermitian) and has pairs of real eigenvalues  $\pm \omega_{n=1 \dots N}$ , where the  $\omega_n > 0$  are the of the Bogoliubov modes of  $H_{\text{MF}}$ . The ground state energy of  $H_{\text{MF}}$  is given by

$$E_{\text{MF}} = \sum_n \omega_n + \sum_{ij} J_{ij} |A_{ij}|^2 + (2S + 1) \sum_i \lambda_i \quad (15)$$

(remark: in a large- $N$  formalism, this corresponds to the energy *per flavor*).

The self consistency is reached when  $A_{ij} = \langle \hat{A}_{ij} \rangle_{GS}$ , which is equivalent to  $\partial E / \partial A_{ij} = 0$ , where  $E$  is the energy of the ground state of  $H_{\text{MF}}$ . The average number of boson per site is equal to  $2S$  (Eq. 4) at the

point(s) where  $\partial E/\partial \lambda_i = 0$ . Since  $\partial^2 E/\partial \lambda^2 \leq 0$  (see this footnote<sup>28</sup>), this point corresponds to a *maximum* of  $\{\lambda_i\} \mapsto E[\{A_{ij}\}, \{\lambda_i\}]$ . For fixed  $\{A_{ij}\}$ , this allows to use a maximization algorithm to determine the chemical potentials  $\lambda_i[\{A_{ij}\}]$ . In a similar way, the self-consistent  $\{A_{ij}\}$  correspond to a *minimum* of  $E[\{A_{ij}\}, \lambda_i[\{A_{ij}\}]]$ .

### A. Gauge invariance and fluxes

The solution of this system of equations is not unique, at least because of the  $U(1)$  gauge invariance of the Hamiltonian. Under the gauge transformation

$$\begin{aligned} b_{j\sigma} &\rightarrow e^{i\theta(j)} b_{j\sigma} \\ \hat{A}_{ij} &\rightarrow e^{i(\theta(i)+\theta(j))} \hat{A}_{ij} \end{aligned} \quad (16)$$

the physical operators (as  $\vec{S}_i$  or  $H$ ) stay unchanged. In other words, the bond parameters  $A_{ij}$  label the physical state in a redundant way. Using gauge transformations we can fix the phases of some  $A_{ij}$ , without changing any physical observable. This decreases the number of variables to be optimized, and is therefore useful in numerical studies.

The moduli  $|A_{ij}|$  are of course gauge invariant quantities, simply related to the energy. But some combinations of complex phases around closed loops are also gauge invariant. Consider the following operator  $\hat{\mathbb{A}}_{i_1 i_2 \dots i_{2n}}$ :

$$\hat{\mathbb{A}}_{i_1 i_2 \dots i_{2n}} = \hat{A}_{i_1 i_2} (-\hat{A}_{i_2 i_3}^\dagger) \hat{A}_{i_3 i_4} \dots (-\hat{A}_{i_{2n} i_1}^\dagger). \quad (17)$$

This operator is defined on any loop with an even length on the lattice and is manifestly gauge invariant. Its mean field (or large- $N$ ) counter part

$$\mathbb{A}_{i_1 i_2 \dots i_{2n}} = A_{i_1 i_2} (-\bar{A}_{i_2 i_3}) A_{i_3 i_4} \dots (-\bar{A}_{i_{2n} i_1}) \quad (18)$$

gives the flux  $\phi_{i_1 i_2 \dots i_{2n}} = \arg(\mathbb{A}_{i_1 i_2 \dots i_{2n}})$  recently discussed by Tchernyshyov *et al.*<sup>29</sup>

In general, the number of variables (all the moduli, plus some phases) grows with the system size. Since it is quite difficult to perform an exhaustive search for mean field solutions if the number of parameters is extensive, the usual strategy is to decrease the number of bond variables by *assuming* that the ground state solution preserves some (or all) symmetries of the lattice. We will however give some examples where the lowest energy solution spontaneously *breaks* some symmetries.

## III. NUMERICAL METHOD

We describe an algorithm to find saddle points (self-consistent mean field state), local minima, and (hopefully) global energy minima.

### A. Determination of the chemical potentials

For given values of the bond parameters  $A_{ij}$ , one should first adjust the chemical potentials ( $\lambda_i$ ).

The basic idea is to perform a (non-linear) least-square minimization of  $\sum_i f_i^2$ , where  $f_i(\{\lambda_i\}) = \langle \hat{n}_i \rangle - \kappa$  is a function of the chemical potentials.<sup>30</sup> Since each density  $\langle \hat{n}_i \rangle$  is an increasing function of  $\lambda_i$ , this method converges relatively rapidly. To do so, we use an implementation of the Levenberg-Marquart algorithm.<sup>30</sup> To make the method faster, we provide the gradient matrix  $G_{ij} = \frac{\partial \langle \hat{n}_i \rangle}{\partial \lambda_j}$  explicitly.  $G_{ij}$  is easy to compute using linear-response theory (using the matrix which implements the Bogoliubov transformation, as well as the energies  $\omega_i$ ). The iterative minimization should start in a region of the space of  $\lambda$  where the Bogoliubov transformation exist ( $M > 0$ ). If the previous values of  $\lambda$  do not satisfy this condition with the new  $\{A_{ij}\}$ , one starts the least-square minimization of  $\sum_i f_i^2$  from a sufficiently low uniform  $\lambda$ .

Finally we note that for some values of the bond parameters  $A_{ij}$ , there is no uncondensed state satisfying  $\langle \hat{n}_i \rangle = \kappa$ . If such a situation is encountered, we add some artificial energy penalty so that the energy-minimization algorithm (next section) tends to escape this point.

### B. Optimization of the bond parameters $A_{ij}$

Equipped with a procedure to compute the  $\lambda_i$  as a function of the  $A_{ij}$ , we can start to look values of  $A_{ij}$  which correspond to self-consistent mean field states. The first stage is simply to iterate the bond self-consistency conditions in the usual way:

- 0 We start from initial random bond values (or perturbing a previously found solution).
- 1 After adjusting the  $\lambda$  by the procedure above, the ground state is obtained by Bogoliubov transformation, and the expectation values  $\langle A_{ij} \rangle$  are computed.
- 2 The bond parameters are replaced by the values above. The new bond parameters are gauge-transformed to a fixed gauge choice where a maximum number of bond parameters are set to be real. This avoids some possible slow drift of some complex phases of the  $A_{ij}$  which would be non-physical.
- 3 Go back to step 2 until the bond parameters do not change by more than a small threshold  $\epsilon$ .

This method was used by Hermele *et al.*<sup>21</sup> in a similar context. It is easy to check that local minima are attractive for these iterations while local maxima are repulsive. More precisely, the error will decrease (resp. increase) in the directions corresponding to eigenvectors of the Hessian (anticipating on Eq. 20) with positive (resp. negative) values. The convergence is faster if the Hessian

eigenvalues are large and positive. In practice, the iterations above allows to quickly go down in energy, but it is not efficient to achieve a full convergence when the system has more than  $\sim 10$  bonds or so. Indeed, it turns out that a high accuracy is required to resolve the possibly small differences (bond modulations, etc) between different saddle points (kagome case in particular, Sec. IV C).

To find accurately self-consistent state, the second stage amounts to perform a least-square optimization on  $\sum_{ij} g_{ij}^2$ , where  $g_{ij}(\{A\}) = \langle \hat{A}_{ij} \rangle - A_{ij}$  is a function of the bond parameters. Of course, the expectation values  $\langle \hat{A}_{ij} \rangle$  are computed after the  $\lambda_i(\{A\})$  have been determined. This second stage allows to converge not only to local extrema but to saddle points as well. Again, we use a Levenberg-Marquart minimization algorithm, with explicit calculation of the gradient  $\frac{\partial \langle \hat{A}_{ij} \rangle}{\partial A_{kl}}$ . The later is again obtained using linear-response theory, with the additional complexity that it contains some terms coming from the variation of the  $\lambda$  :

$$\left. \frac{\partial \langle \hat{A}_{ij} \rangle}{\partial A_{kl}} \right|_{\langle \hat{n} \rangle = \kappa} = \left. \frac{\partial \langle \hat{A}_{ij} \rangle}{\partial A_{kl}} \right|_{\lambda \text{ fixed}} + \sum_{a,b} \frac{\partial \langle \hat{A}_{ij} \rangle}{\partial \lambda_a} \left[ \frac{\partial \langle \hat{n} \rangle}{\partial \lambda} \right]_{ab}^{-1} \frac{\partial \langle \hat{n}_b \rangle}{\partial A_{kl}} \quad (19)$$

As for the first stage, we work with bond variables corresponding to a fixed gauge choice. In particular, the matrix of Eq. 19 is evaluated in the subspace of bond parameter variations which is orthogonal to pure gauge transformations. This is important to get rid of unphysical slow phase drifts during the iterations. Most of the time a double precision accuracy is reached in less than 10 Levenberg-Marquart iterations when the system has less than one hundred bonds or so.

Finally the optimization is repeated using at least a few hundred (often thousands) of random initial conditions for the  $A_{ij}$ . This is relatively time consuming since each evaluation of the energy (or its derivatives) requires a numerical adjustment of the chemical potentials (Sec. III A), which is itself a (convex) least-square problem with many variables.

Varying the parameter  $\epsilon$  (stopping criterion for the iterations of stage 1) allows to tune if the method will converge toward very low-energy saddle points (small  $\epsilon$ ), or saddle point at higher energy (larger  $\epsilon$ ). If  $\epsilon$  is very small (say  $10^{-5}$ ) the first stage will terminate close to the ground state and the second step (least-square) will converge to the ground state with high probability if the system is not too large ( $\lesssim 100$  bonds). On the other hand, if  $\epsilon$  is too large, the first stage will stop at some relatively high energy configuration. In such region of the  $A$  space we expect a very (exponentially) high density of saddle points. In practice this density of saddle point is so high that the program will find a new solution at every run, and a given saddle point will rarely be obtained twice. The best choice is to adjust  $\epsilon$  so that the iteration stage leads to configurations in a typical energy

range above the ground state where the number of saddle points is not too large (a few tens). In such a case, after a sufficiently large number of runs, one obtains the full (or almost full) list of saddle points in that energy window. Of course, due to the large number of variables, one cannot exclude the presence of some additional saddle points with a small basin of attraction with respect to this algorithm.

### C. Hessian and stability

The least-square procedure described above leads to self-consistent mean field states, satisfying  $A_{ij} = \langle \hat{A}_{ij} \rangle$ . These states are saddle point of the energy (considered as a function of the  $A_{ij}$ , and the chemical potential being themselves functions of the  $A_{ij}$ ). To check if each mean field state is a local minimum, local maximum, or generic saddle points with stable as well as unstable directions, we compute the Hessian matrix:

$$K_{l,l'} = \frac{\partial^2 E_{\text{MF}}}{\partial A_l^\epsilon \partial A_{l'}^{\epsilon'}} = 4J_l \left( \delta_{ll'} \delta_{\epsilon\epsilon'} - \left. \frac{\partial \langle \hat{A}_l^\epsilon \rangle}{\partial A_{l'}^{\epsilon'}} \right|_{\langle \hat{n} \rangle = \kappa} \right) \quad (20)$$

where  $l$  and  $l'$  represent two bonds and  $\epsilon$  and  $\epsilon'$  denote the real or Imaginary part of the bond variables (see Eq. 19 for derivatives of the bond expectation values at fixed densities).

Due to the gauge invariance of the model, the Hessian contains some zero eigenvalues associated to infinitesimal gauge transformations. The number of such gauge modes can be computed on each given lattice (using the rank of a modified adjacency matrix of the lattice<sup>31</sup>), and these non-physical zero eigenvalues are of course be discarded when discussing these solutions. For the clusters studied here, the number of zero eigenvalues is always equal to the number of pure gauge modes, so we can conclude that there is no *physical* zero mode in the Hessian. The sign of the smallest non-zero eigenvalue of  $K$  tells us whether the mean field state is a local minimum, or an unstable saddle point.

The spectrum of the Hessian for the ground state gives some information about the magnitude of the  $1/N$  corrections due to Gaussian fluctuations in the vicinity of the energy minimum. Finally, the spatial structure of the lowest eigenvector of the Hessian gives some information about the nature of these fluctuations.

## IV. NUMERICAL RESULTS

### A. Square lattice

The SBMFT phase diagram is well known on the square lattice: magnetic long-range order for  $\kappa \gtrsim 0.39$ <sup>7</sup> and a disordered phase with gapped spinons for  $\kappa \lesssim 0.39$  ("Coulomb" phase, unstable at finite- $N$ <sup>6</sup>). In the ordered



phase the spinon gap drops as  $\sim 1/N_s$  ( $N_s$  is the number of sites) and Bose-condensation occurs in the thermodynamic limit, leading to spontaneous break down of the spin rotation symmetry. By considering here only finite clusters, the ground state is always rotationally invariant and the gap finite. Still, both phases can be distinguished using standard finite size-scaling for the gap or spin-spin correlations. We will discuss how the “energy landscape” of mean field saddle points differ between the two phases.

### 1. Hessian of the ground state and gauge modes

We did some extensive search for saddle points on square lattices with 36 sites and with  $\kappa = 2S = 0.1$  and  $\kappa = 1$ . The ground state, as expected, is spatially uniform, real, and has a vanishing flux on all the square plaquettes, whatever the boson density. However, the spectrum of the Hessian is quite different in the magnetic phase and in the disordered phase.

In Fig. 1 the smallest eigenvalue of the Hessian (Eq. 20) is plotted as a function of the “spin”  $S$ , for different system sizes (up to 144 sites). Although finite-size effects are important, these data indicate that the Hessian is gapped in the thermodynamic limit for large  $S$ , while it becomes gapless for small  $S$ . The transition very likely coincides with that of magnetic long-range order.

The gaplessness of the Hessian in the disordered region is due to the bipartite character of the lattice. On a bipartite lattice, the bond parameters are invariant under *staggered* gauge transformations:

$$b_{r\sigma} \longrightarrow b_{r\sigma} e^{i(-1)^r \theta} \quad (21)$$

$$A_{rr'} \longrightarrow A_{rr'} \quad (22)$$

which, in Wen’s terminology,<sup>32</sup> means that the invariant gauge group (IGG) is  $U(1)$ .

If we perform a spatially varying gauge transformation including the staggered factor we get

$$b_{r\sigma} \longrightarrow b_{r\sigma} e^{i(-1)^r \theta(r)} \quad (23)$$

$$A_{rr'} \longrightarrow A_{rr'} e^{i(\theta(r) - \theta(r'))}, \quad (24)$$

where  $r$  (resp.  $r'$ ) is on the even (resp. odd) sublattice. Starting from a state described by  $A_{rr'}^0$ , we construct a phase fluctuation of the bond parameters parametrized by  $a_{rr'} \in \mathbb{R}$ :

$$A'_{rr'} = A_{rr'}^0 + dA_{rr'} = A_{rr'}^0 e^{ia_{rr'}} \quad (25)$$

From Eq. 24,  $a_{rr'}$  transforms as a conventional  $U(1)$  gauge field:

$$a_{rr'} \longrightarrow a_{rr'} + \theta(r) - \theta(r'). \quad (26)$$

So, if we denote by  $E(\{a_{rr'}\})$  the energy of the perturbed mean field state (after the appropriate adjustment of the chemical potentials), the energy should be gauge invariant under Eq. 26.

In the small- $S$  phase where the bosons are gapped and their correlation length is short,  $E(\{a_{rr'}\})$  should be a local function of the fluctuation  $a_{rr'}$ .

The simplest local term compatible with gauge invariance would be the lattice version of the magnetic energy  $(\vec{\nabla} \times \vec{a})^2$ , and would take the form of the square of the circulation of  $a$  around small loops (this can also be obtained from a small- $S$  expansion<sup>29</sup>). This would give an Hessian eigenvalue scaling as the square of the smallest available wave-vector, that is  $\sim 1/L^2 \sim 1/N_s$  ( $L$  the linear size and  $N_s$  the number of sites). Such modes are indeed found in the spectrum of the Hessian and correspond to the *second* non-zero eigenvalue. The associated eigenvector is displayed in Fig. 2. The thickness of each bond  $l$  is related to the modulus  $|dA_l|$  while the color represents the complex argument of  $dA_l/A_l$ . In the present case, these complex arguments take only two values:  $\pm\pi/2$  (blue and yellow), indicating that  $dA$  is a *gauge mode* of the form of Eq. 25, with  $dA_l/A_l^0 \sim ia_l \in i\mathbb{R}$ . In the present case  $a_l \sim \cos(2\pi x_l/L)$  for a vertical link  $l$  (oriented from the even to the odd sublattice) at horizontal position  $x$ , and  $a_l = 0$  on horizontal bonds. This gauge model may be viewed as a low-energy “photon” of the effective gauge theory.<sup>6</sup>

In fact the numerical data indicate that the *lowest* eigenvalue of the Hessian decays *faster* than  $1/N_s$  (Fig. 1). The associated mode is represented in Fig. 3, and is also a gauge mode ( $dA_l/A_l^0$  is purely imaginary). Inspecting the sign of  $a_l$  one sees that it corresponds to a change in the “global” flux associated to the large loops encircling the torus while local loops are unaffected by this gauge mode. The structure of this eigenvector of the Hessian turns out to be the same for all system size, and does not depend on the spin value. We expect its eigenvalue to decay exponentially with the system size in the small- $S$  phase.

In the Néel phase,  $E(\{a_{rr'}\})$  need not be short-ranged and the arguments above fail. Indeed, the spinon are charged particles for the gauge field and their condensation gaps out the gauge degrees of freedom (Anderson-Higgs mechanism). In the Néel phase, computing the boson energy in presence of a global flux (through loops encircling the torus) amounts to impose some twist on the spin directions and the finite spin stiffness  $\rho$  naturally leads to an energy cost proportional to the square of the flux, and leads to a finite Hessian eigenvalue proportional to  $\rho$ . In turn, the finite Hessian gap in the Néel phase indicates a relative stability of the mean field state with respect to Gaussian  $1/N$  corrections.

### 2. Excited mean field solutions for $\kappa = 1$ .

For  $\kappa = 1$  (Néel phase), our search for saddle point on the 36 site cluster shows that the ground state ( $-30.93605205126$ ) is well separated from the first excited saddle point ( $E = -28.82425530821$ , Fig. 4). No local minimum was found at low energy (see Tab. I), but

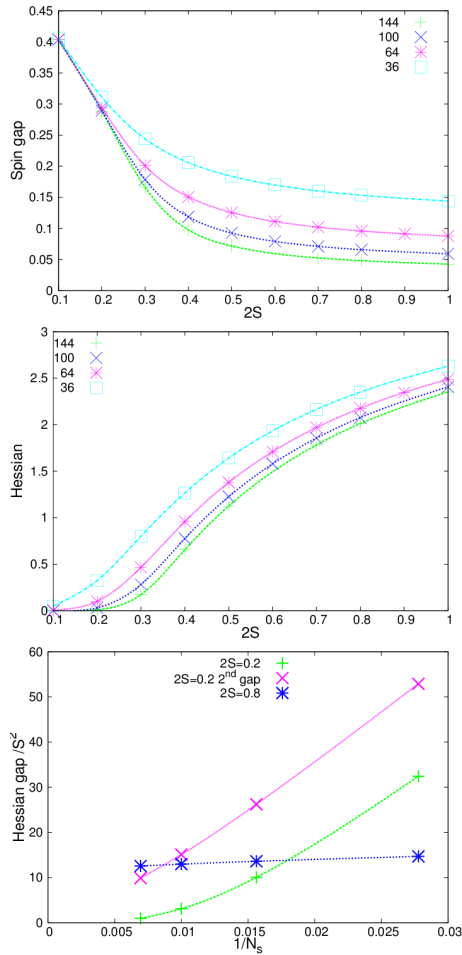


FIG. 1: Square lattice model. Top: spin gap as a function of  $\kappa = 2S$ . In the thermodynamic limit this state is associated to magnetic long-range order (vanishing spin gap) for  $2S > S_c \simeq 0.39$ .<sup>7</sup> Middle panel: smallest eigenvalue of the Hessian for the ground state on 36, 64 and 144-site square lattices. Bottom: scaling of the lowest Hessian eigenvalue as a function of the system size  $N_s$ . This shows that the Hessian is gapless for  $2S = 0.2$  and gapped for  $2S = 0.8$ . The Hessian gap is presumably finite in the magnetic phase, while it is likely to vanish in the thermodynamic limit for  $S < S_c$ . For  $2S = 0.2$ , first eigenvalues decays faster than  $1/N_s$  whereas the second eigenvalue goes to zero as  $\sim 1/N_s$  (see text).

only saddle points. In addition, the excited saddle points turn out to have very unstable directions (strongly negative Hessian eigenvalues). There might be some other mean field states in the energy range of Tab. I, but these should have rather small basin of attraction with respect to our search algorithms, since this list of the twelve lowest energy state is stable after thousands of runs starting from random initial conditions.

The first excited saddle point is displayed in Fig. 4. It takes the form of an excitation localized around one site (here site number 14). This state is chiral, with a flux equal to  $\pm 0.40461332\pi$  on the four square plaquettes touching the center of the excitations. The flux then

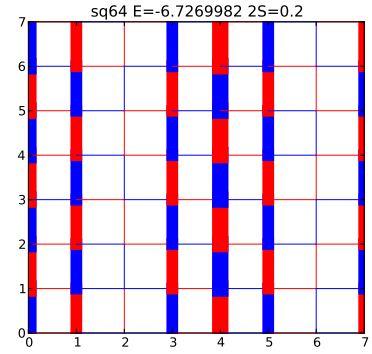


FIG. 2: Hessian eigenvector  $dA_l$  corresponding to the second smallest eigenvalue (0.26224396339) for a 64-site square lattice with  $S = 0.1$ . The thickness of each bond  $l$  is proportional to the modulus  $|dA_l|$  while the color represents the complex argument of  $dA_l/A_l$ . Red: argument is  $+\pi/2$ , blue is  $-\pi/2$ . Here  $dA$  is a gauge excitation, it corresponds to a long wavelength modulation of the flux through each plaquette. Here the wave-vector is parallel to the horizontal bonds. This gauge mode is associated to the smallest non-zero wave vector on the square lattice and is therefore four-fold degenerate.

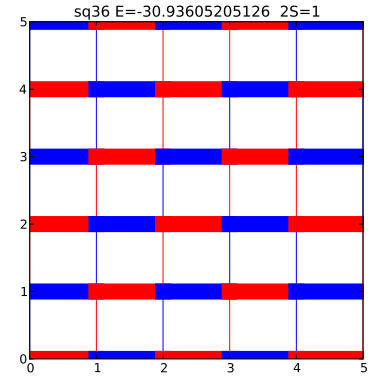


FIG. 3: Hessian eigenvector  $dA_l$  corresponding to the smallest eigenvalue (2.62955994344) for a 36-site square lattice. Same representation as in Fig. 2. The complex argument of  $dA_l/A_l$  takes only two values:  $\pm\pi/2$  (blue and red), indicating that  $dA$  is a gauge excitation. This mode corresponds to an increase of the flux through large horizontal loops, and no change for the flux going through local plaquettes.

decreases quickly with distance (see caption of Fig. 4), but the fact that some non-trivial fluxes (different from 0 or  $\pi$ ) around the center of the excitation shows that it induces some non-coplanar spin-spin correlations. Far from the center of the excitation the spins remain in a collinear and in an ordered structure. The center spin is correlated with its neighbors, but it is very weakly correlated ( $\langle \vec{S}_{14} \cdot \vec{S}_i \rangle \simeq 0$ ) with the site which are far apart. Interestingly, a similar excitation is found in the ordered phase of the triangular lattice.

$E$	$\Delta$	$H$	$d$	$N_\lambda$	$\min_\lambda$	$\max_\lambda$	$N_{ A }$	$\min_{ A }$	$\max_{ A }$	
-30.93605205126	0.14402872021	2.6295599434	1	1	-2.33625413623	-2.33625413623	1	0.58295256650	0.58295256650	R
-28.82425530821 <sup>a</sup>	0.12128968489	-7.7009935434	36	10	-2.35767326534	-0.80802876988	12	0.46297459737	0.58363641125	C
-28.78219048843	0.10001664198	-50.5062824348	72	13	-2.36085237706	-0.70467719552	18	0.45635222273	0.59393955633	R
-28.36943538503	0.15018056150	-26.9056949522	72	12	-2.37180295956	-1.25427516482	25	3.06482822239e-15	0.78318014761	C
-27.87811171341	0.10635799592	-48.4908669283	72	12	-2.37611640988	-1.20158916706	18	0.33406678717	0.62744479349	R
-27.67404431445 <sup>b</sup>	0.24030790672	-33.3227937772	2	1	-2.12079971339	-2.12079971339	2	0.52769740399	0.59657118301	R
-27.58542591653	0.12018732985	-11.9733712946	72	16	-2.38843405218	-1.28794576300	24	0.29836817056	0.63116481780	C
-27.55178404956	0.08439099361	-67.0253600361	72	16	-2.48677863782	-1.13200578463	24	3.38069859599e-16	0.64685457030	C
-27.52461818853	0.19788831856	-3.8580290414	36	6	-2.23233357411	-1.87795360324	14	0.45547996236	0.59859663572	C
-27.49457258263	0.18888774623	-1.9063958450	36	8	-2.24866064506	-1.74743986196	14	0.46141122781	0.60087012841	C
-27.49456554040	0.19367584933	-5.7251545034	36	6	-2.22476689000	-1.75751056646	14	0.34656259228	0.60092322028	C
-27.40385237877	0.16760744308	-21.1217748777	144	18	-2.32248736876	-1.30042949863	38	0.27024089067	0.64068344661	C

TABLE I: Low-energy saddle points for a square lattice cluster with 36 sites and  $S = 0.5$ . From the left column to the right: energy, spinon gap, lowest non-zero Hessian eigenvalue, degeneracy, number of different chemical potentials  $\lambda$  (1 means uniform, etc.), minimum and maximum values of  $\lambda$ , number of different values of  $|A|$  minimum and maximum values of  $|A|$ , real (R) or complex/chiral solution (C). The spatial modulations of  $|A_{ij}|$  and  $\lambda_i$  for solution <sup>a</sup> are displayed in Fig. 4. Solution <sup>b</sup> has the same spatial structure (two-fold degeneracy) as the one shown in in Fig. 6b.

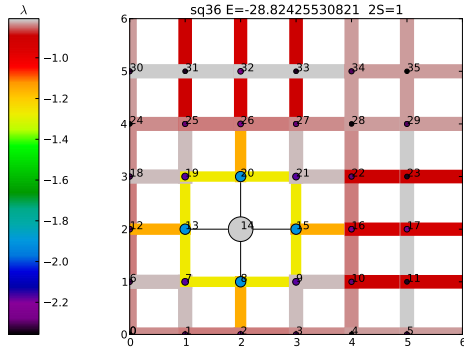


FIG. 4: First excited mean field solution on a square lattice with 36 sites and  $S = 0.5$ . The modulus of the bond parameter (right color scale) is indicated, as well as the chemical potentials (left scale). This solution shows a localized excitation (here around site number 14). The flux decays rapidly with distance from the center:  $0.4046133\pi$  on plaquette  $[8,9,15,14]$ ,  $0.037028\pi$  on plaquette  $[1,2,8,7]$ ,  $-0.005291300\pi$  on  $[0,1,7,6]$ ,  $0.0001131\pi$  on  $[4,5,11,10]$ , etc. See Fig. 5 for some the spin-spin correlations in this state.

### 3. Excited mean field solutions for $\kappa = 0.1$ .

For  $\kappa = 0.1$ , the ground state on the square lattice is still uniform and without any flux, but the spinon gap (Fig. 1) remains finite in the thermodynamic limit. This mean field state has been argued<sup>6</sup> to be unstable at finite  $N$ , due to strong gauge fluctuations. The finite  $N$  ground state is believed to spontaneously break some lattice symmetry to form a valence-bond crystal. In fact, the mean field energy landscape is very different from the one observed in the magnetic phase. The first local minima and saddle points are listed in Tab. IV A 3.

We observed a high density of local minima and saddle points, with very small Hessian eigenvalues. This high density of excited saddle points reflects the presence of some strong gauge fluctuations at (large but) finite  $N$ . We note that several such saddle points display modu-

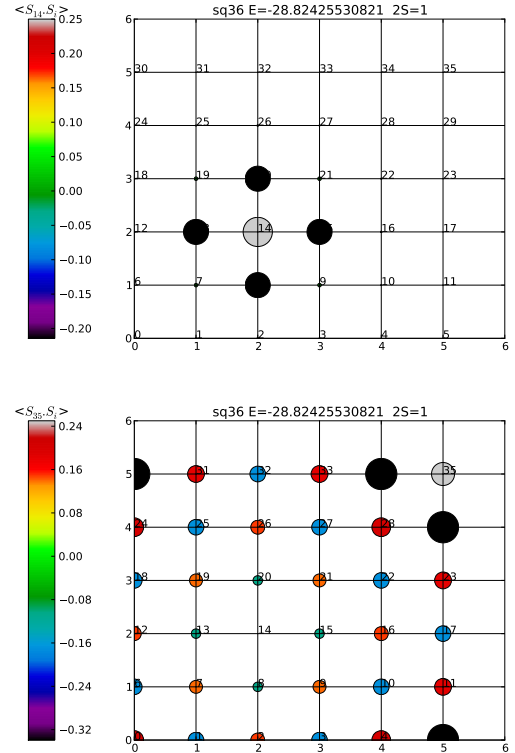


FIG. 5: Spin-Spin correlation in the first excited of a 36-site square lattice with  $S = 0.5$  (same state as in Fig. 4). The radius of the circle on site  $j$  proportional to the correlation  $|\langle \vec{S}_{i0} \vec{S}_j \rangle|$  with the reference site  $i_0$  (the sign is available on the color scale). Top: the reference spin  $i_0 = 14$  is at the center of the localized excitation. Bottom: the reference spin  $i_0 = 35$  is “far” from the center of the excitation.

lations of the bond amplitudes  $|A|$  which have the same symmetries as the valence-bond crystals previously considered for square lattice antiferromagnets. The first excitations (line <sup>a</sup> in Tab. IV A 3) shows a one-dimensional modulation, which is predicted to occur at finite  $N$  when  $\kappa = 2 \bmod 4$ .<sup>6</sup> And among the highly symmetric so-

$E$	$\Delta$	$H$	d	$N_\lambda$	$\min_\lambda$	$\max_\lambda$	$N_{ A }$	$\min_{ A }$	$\min_{ A }$	
-1.83492169860	0.40562447718	0.0514862091	1	1	-0.62322660824	-0.62322660824	1	0.11828994799	0.11828994799	R
-1.83349695884 <sup>a</sup>	0.43766690295	-0.0513757991	2	1	-0.62174106995	-0.62174106995	2	0.11707639293	0.11940834877	R
-1.83265972180	0.42301616405	3.3891521814e-05	36	6	-0.62283957972	-0.61901747505	12	0.11749362973	0.11895083747	C
-1.83265969367	0.42301757051	-3.3879532685e-05	72	12	-0.62289751868	-0.61872552844	25	0.11742978176	0.11900687718	C
-1.83265966553	0.42301846049	-3.3877477372e-05	36	10	-0.62295399258	-0.61842513968	12	0.11745616476	0.11898150831	C
-1.83162471056	0.41456789451	-0.2513880759	36	6	-0.62576828556	-0.60318829800	12	0.10370572327	0.13006171701	C
-1.83121683711	0.41375814481	-0.2872095650	72	12	-0.63567288324	-0.58931901135	25	0.03077944153	0.13945180759	C
-1.83088353771	0.43032855876	-0.2737625727	72	9	-0.62660943591	-0.60282776054	24	0.10017310034	0.13081740450	C
-1.83047599540	0.42976957584	-0.3191268237	72	12	-0.63670770779	-0.58921985280	25	0.01544819043	0.13979752631	C
-1.83036799495	0.43107796748	-0.3414892108	72	12	-0.63601360482	-0.58745590945	25	0.00522910878	0.14104278833	C
-1.83004203619	0.43897814318	-0.2774384716	36	6	-0.62530891168	-0.60252710044	12	0.10277137746	0.13077306110	C
-1.82976553423 <sup>c</sup>	0.44236450064	0.0004197766	9	3	-0.62142264885	-0.61823831215	4	0.11796026878	0.11822830533	C
...										
-1.82534862050 <sup>b</sup>	0.45598298556	0.0049547827	4	1	-0.61651000360	-0.61651000360	2	0.11510636037	0.12084117665	C

TABLE II: Low-energy saddle points for a square lattice cluster with 36 sites.  $S = 0.05$ . Solutions <sup>a</sup> and <sup>b</sup> are displayed in Fig. 6, and solution <sup>c</sup> is shown in Fig. 7.

lutions we also note a plaquette valence-bond crystal (VBC) ( $E = -1.82534862050$ ) (Fig. 6). This state does however not correspond to a simple VBC since it is a complex/chiral solution with non-trivial (different from 0 or  $\pi$ ) fluxes on all the square plaquettes. See also Fig. 7 for another VBC-like state. According to the analysis of Read and Sachdev, non-perturbative gauge fluctuations (proliferation of hedgehogs point-like instantons) are responsible for the lattice symmetry breaking at finite  $N$ , leading to a modulation of  $|A|$  which is exponentially small in  $N$ . The mechanism is somewhat different here since we observe VBC-like low-energy saddle points although gauge fluctuations are completely absent ( $A_{ij}$  is frozen in the SBMFT). In Sec. IV C we will also report a case where the ground state itself exhibits some spontaneous bond amplitude modulations.

## B. Triangular lattice

### 1. Hessian of the ground state

On the triangular lattice we find that the lowest energy state corresponds to the (spatially uniform) solution studied by Sachdev<sup>9</sup> (0-flux state<sup>14</sup>) and leads to magnetic long-range order ( $\sqrt{3} \times \sqrt{3}$ ) for  $2S > 0.34$ , and a gapped and deconfined  $\mathbb{Z}_2$  liquid for  $2S \lesssim 0.34$ . As usual, these two phases can be distinguished by the spinon gap: it drops to zero when increasing the system size in the magnetic phase and stays finite in the liquid phase (see Fig. 8).

The Hessian has a large lowest eigenvalue, which indicates the stability of this mean field state with respect to  $1/N$  fluctuations. The evolution of this lowest eigenvalue is plotted in Fig. 8. It slightly decreases with the system size (comparing 36 and 144 sites), but is certainly finite in the thermodynamic limit. Contrary to the square lattice situation, one does not detect any dramatic change of behavior between the gapped phase and the magnetic one.

In fact, since the lattice is no bipartite, the IGG of the uniform mean field state is discrete ( $\mathbb{Z}_2$ ) and we do

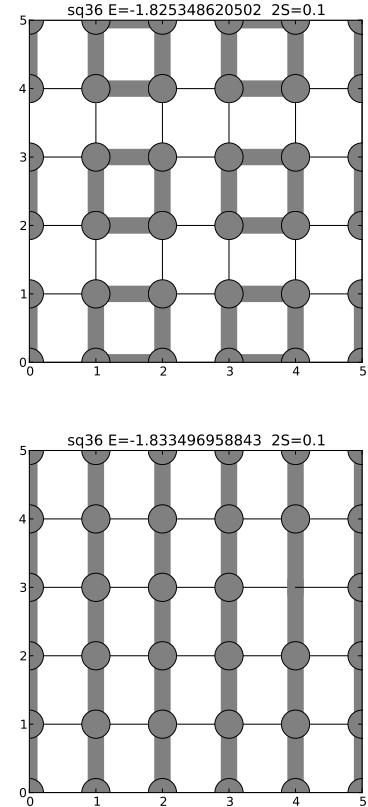


FIG. 6: Two low-energy mean field solutions on a square lattice with 36 sites and  $S = 0.05$ .  $|A|$  takes only two values and the bonds with the stronger  $|A|$  are indicated by fat grey lines (for values, see Tab. IV A 3). All the sites are equivalent and the chemical potential is uniform in both cases.

not expect any gapless modes associated to *small* perturbations  $A_{ij} = A_{ij}^0 + dA_{ij}$  with  $|dA_{ij}| \ll 1$ . Still, important  $\mathbb{Z}_2$  (gapped) gauge excitations are expected in the spin liquid phase, and they will be discussed in Sec. IV B 3.

The lowest eigenvector of the Hessian is represented in Fig. 9 for  $S = 0.05$ . As in all the cases we looked at, it



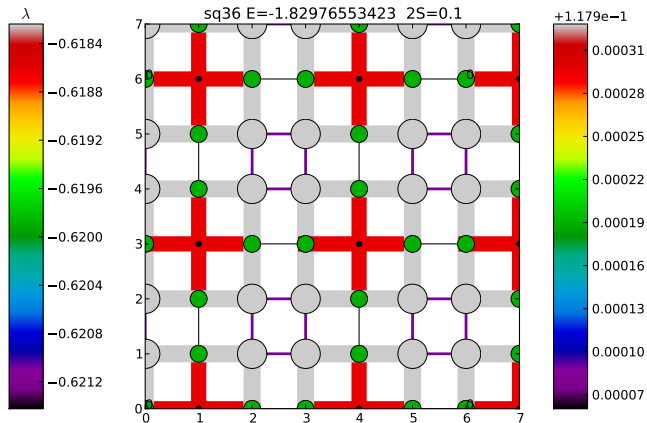


FIG. 7: A low-energy mean field solution on a square lattice with 36 sites and  $S = 0.05$ . The modulus of the bond parameters is indicated – the right color scale shows deviations from the minimum value. The left color scale indicates the chemical potentials (dot on each site). This solution shows modulations with the symmetries of a 3-cell VBC.

correspond to a *phase* fluctuation of the bond variables. The associated flux modulations for all diamond loops are shown in the bottom panel of the figure (note that the sign of each flux is somehow arbitrary since it depends on the choice of an origin of the loop).

## 2. Excited mean field solutions

In Tab. III we list these first mean field states obtained for  $S = 0.5$  in a 36-site sample. As for the square lattice in its magnetic phase, we only find saddle points and no local minima among the first states. The first excited saddle point is at an energy 0.94927 above the ground state and this gap is very likely finite in the thermodynamic limit. This excited state has the spatial structure of a localized excitations (Fig. 10) which resembles that of the square lattice. Finally, we note that contrary to the square lattice case, the lowest energy states of Tab. III have real bond amplitudes (more precisely: can be made real with an appropriate gauge choice), indicating the coplanar nature of their spin-spin correlations.

For small enough  $\kappa = 2S$ , the SBMFT describes a gapped spin liquid of  $\mathbb{Z}_2$  type.<sup>9,14</sup> Tab. IV gives the first saddle points obtained at  $2S = 0.1$ . The ground state is uniform and all the rhombi have a vanishing flux, as expected. The first excited saddle point has slight modulations ( $\sim 6.10^{-4}$ ) of the bond amplitudes (Fig. 11). This state also has vanishing fluxes on all the rhombi, but it differ from the ground-state by the presence of an additional flux  $\pi$  along some long loop winding around the torus (three possible choices). These three states become homogeneous in the thermodynamic limit and degenerate with the ground state. With the ground state they

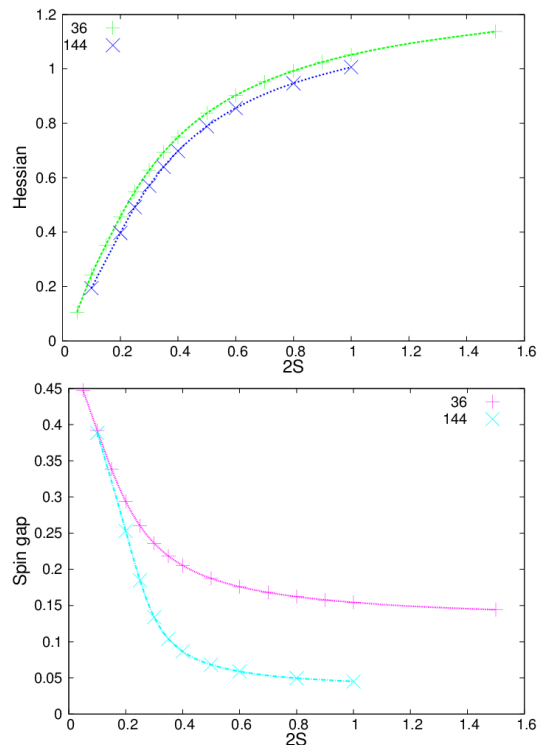


FIG. 8: Top panel: smallest eigenvalue of the Hessian for the ground state state on 36-site and 144-site triangular clusters. Bottom: spin gap. In the thermodynamic limit this state is associated to magnetic long-range order (vanishing spin gap) for  $2S \gtrsim 0.34$ .<sup>9</sup>

form the four-fold topological degeneracy of the  $\mathbb{Z}_2$  liquid on a torus.<sup>3,33</sup> These states were found by the optimization algorithm starting from random initial conditions, and not “forced” by hand. We are thus confident that the method is able to find the low energy solutions in a systematic way on small clusters at least up to a few tens of sites and bonds.

Above the four topological ground states we observe a many saddle points which do not show any simple spatial pattern (high number of inequivalent sites and bonds). These states have energies significantly below the first vison-pair state we have found (last line in Tab. IV and Fig. 12). Due to the presence of complex fluxes (not 0 or  $\pi$ ) in these states, they may not have any interpretation in terms of the  $\mathbb{Z}_2$  gauge degrees of freedom.

## 3. Visions

A  $\mathbb{Z}_2$  liquid possesses non-magnetic excitations named *visions*, which correspond to  $\pi$ -flux quanta of the effective Ising gauge theory.<sup>6,33</sup> In a finite system (without boundaries) the number of vison is necessarily even, and a trial vison-pair state can be constructed as follows. One starts from the uniform mean field ground state and one reverses the sign of the bond parameters  $A_{ij}$  for all the

$E$	$\Delta$	$H$	d	$N_\lambda$	$\min_\lambda$	$\max_\lambda$	$N_{ A }$	$\min_{ A }$	$\max_{ A }$	
-26.40405992819	0.15424645309	1.0517831524	1	1	-2.58830049633	-2.58830049633	1	0.49723336391	0.49723336391	R
-25.45478884810	0.14039937369	-2.3583827803	36	7	-2.68083518864	-1.66967911414	12	0.41812686812	0.56615895080	R
-24.89782095003	0.13788292075	-2.1218542408	108	12	-2.66775663053	-1.86004294873	31	0.25950830810	0.56907182479	R
-24.88367410179	0.11975325026	-2.3419680753	432	36	-2.76307967976	-1.75626091358	108	0.13936678359	0.57983094362	R
-24.88248919944	0.14303067790	-2.3536310845	216	18	-2.72365738218	-1.77512884614	56	0.18149763138	0.57925175603	R
-24.85225639276	0.05506495561	-2.6494385700	216	21	-2.87033693396	-1.82953713470	57	0.05089520618	0.56602789699	R
-24.54012950533	0.07534371832	-2.7179265074	216	18	-2.83154574151	-1.61720470431	56	0.25139432620	0.57460696668	R
-24.52557412388	0.06458137688	-2.4327487996	216	18	-2.82124110423	-1.87789249232	56	0.09674702612	0.56912072760	R
-24.51689402152	0.10842201321	-2.4288970581	72	10	-2.79081268614	-1.66076773241	21	0.35681606435	0.56617071630	R
-24.42913380032	0.13143243020	-2.5993027532	54	8	-2.66560684707	-1.62001869447	17	0.38239562932	0.56552771557	R
-24.38386557808	0.12833408469	-2.0204356396	108	13	-2.73034611703	-1.88206681620	30	0.25362349993	0.56892183451	R
-24.36651624089	0.11045933281	-2.2168211792	432	36	-2.76253254084	-1.77578363386	108	0.10590160533	0.58136368633	R

TABLE III: Energy minimum and low-energy saddle points for a triangular lattice cluster with 36 sites and  $S = 0.5$ . Notice that the ground state is very stable (large Hessian gap: 1.051) and that all the other saddle points are unstable (negative Hessian eigenvalue). The gap  $-25.454 + 26.404 = 0.949$  is also quite large compared to the kagome case (next section). The ground state ( $E = -26.40405992819$ ) is a solution with vanishing flux on all the diamonds, and three-sublattice long-range spin-spin correlations (the critical value for magnetic long-range order is  $2S = 0.34$ ).<sup>9</sup> The bond strength of the first excited state are displayed in Fig. 10.

$E$	$\Delta$	$H$	d	$N_\lambda$	$\min_\lambda$	$\max_\lambda$	$N_{ A }$	$\min_{ A }$	$\max_{ A }$	
-1.77115513853	0.39183413870	0.2418792448	1	1	-0.63927958247	-0.63927958247	1	0.09721004221	0.09721004221	R
-1.76857445623	0.43969994315	0.1404951036	3	1	-0.63620536809	-0.63620536809	2	0.09694182615	0.09756074413	R
-1.76558449027	0.40008559551	-0.0136673394	108	13	-0.64036695527	-0.61163933625	30	0.08631046645	0.10220320383	C
-1.76556438644	0.39881698544	-0.0662494156	216	21	-0.64094448900	-0.60807754792	57	0.07142251452	0.11045947514	C
-1.76519815707	0.40323866935	-0.0476017475	216	21	-0.64101212209	-0.62149883058	57	0.08166138572	0.10941122095	C
-1.76517640350	0.40348584568	-0.0574617718	432	36	-0.64242077150	-0.62028199544	108	0.08102625728	0.11240116020	C
-1.76512811482	0.40255745524	-0.0675887556	216	21	-0.64418307267	-0.62192577975	57	0.07214207918	0.11553853523	C
-1.76498033616	0.40426965800	-0.0822323880	216	18	-0.64027903292	-0.62235496321	56	0.07818420245	0.11549233664	C
-1.76494386569	0.40647240030	-0.0077675537	108	12	-0.64031335557	-0.61976563929	31	0.08656330909	0.10201782841	C
-1.76490270376	0.41103320490	0.0552851450	216	18	-0.64030870204	-0.62463756694	56	0.08904499619	0.10413653140	C
-1.76486322625	0.40885376933	-0.0517770911	432	36	-0.64144886953	-0.62152076605	108	0.08370457723	0.10627245220	C
-1.76481070231	0.40714839383	-0.0588744760	216	18	-0.64059451058	-0.62076171059	56	0.08285231897	0.10673538608	C
...	...	...	...	...	...	...	...	...	...	...
-1.76267094982	0.41119320956	-0.2136294440	108	12	-0.64647502600	-0.60434357136	31	0.07784772351	0.11384461169	R

TABLE IV: Low-energy saddle points for a triangular lattice cluster with 36 sites and  $S = 0.05$ . The ground state and the first excited saddle point ( $E = -1.76857445623$ , three fold degenerate) form the four-fold topological degeneracy.<sup>3,33</sup> The other saddle points listed here are chiral(complex), except for the last line, which corresponds to a pair of visons (see Sec. IV B 3 and Fig. 12).

bonds  $ij$  crossing a cut extending from the a first plaquette to a second one. The gauge flux is then concentrated in the immediate vicinity of these two plaquettes which correspond to the vison core positions. Any gauge-invariant operator far from the vison cores is unaffected by this modification.

Due to the presence of flux  $\pi$  for each loop encircling a vison core, such a trial state is in general not self-consistent ( $\langle \hat{A}_{ij} \rangle \neq A_{ij}$  and  $\langle \hat{n}_i \rangle \neq \kappa$ ). To obtain a self-consistent state (saddle point) the bond moduli as well as the chemical potentials should be re-adjusted in the vicinity of the vison cores. We obtain numerically such self-consistent vison-pair states by looking at the nearest saddle point in the vicinity of the trial state (second stage of the algorithm described in Sec. III B). These gives access to some energetics of the visons, and to their energy as a function distance in particular.

Typical vison-pair solutions are displayed in Fig. 12 and Fig. 13. The modulation of  $|A|$  in the vicinity of each vison is clearly visible, as well as the higher (less negative) chemical potentials in the core regions. In this case ( $S = 0.1$ ) the vison core radius is of the order of two lattice spacings. These excited states are however not local minima, but saddle points. In all the cases considered here (vison distance from 2 to  $4\sqrt{3}$ ) we find

four negative Hessian eigenvalues, with a rather weak dependence on the vison separation.

A calculation of the bond modulations in a vison mean-field state was recently carried out by Huh, Punk and Sachdev<sup>34</sup> using an effective model valid in the limit of large spinon gap. Their result indicates that  $|A_{ij}|$  decreases on all the bonds close to the vison core. In our calculation it appears that the some moduli are indeed depressed, but some are also enhanced (red bonds in Fig. 12 and grey bonds in Fig. 13).

Some aspects of the visons energetics are summarized in Fig. 14. In the large- $N$  framework, these energies should be multiplied by a factor  $N$ . It can be checked that their mutual interaction is very weak, since the total energy hardly depends on the distance, as expected in a gapped  $\mathbb{Z}_2$  liquid phase. These calculations also provide some information about the spinon-vison interactions. This question is important since vison-spinon bound states have fermionic mutual statistics.<sup>33</sup> It appears however that the spinon gap  $\Delta$  is slightly *higher* in presence of a vison pair than in the ground state ( $\Delta_0$ ). This indicates some vison-spinon repulsion and makes unlikely the existence of a bound-state between these two excitations.

We investigated the effect of inserting two  $\pi$  fluxes far

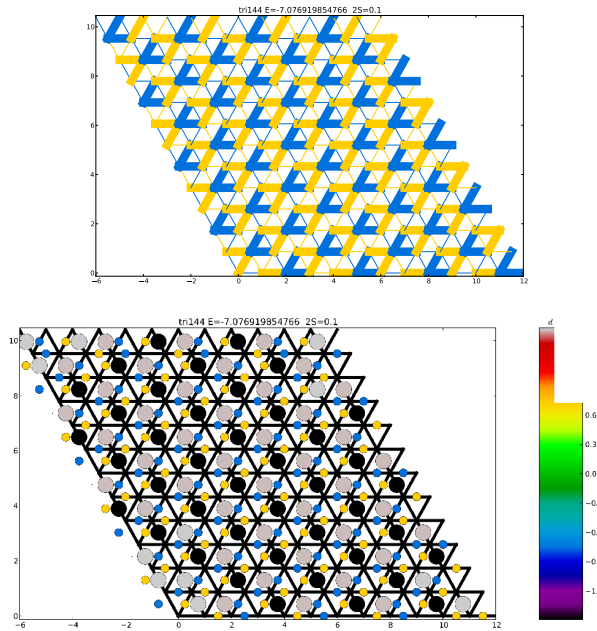


FIG. 9: Hessian eigenvector  $dA/A$  corresponding to the smallest (degenerate) eigenvalue (0.1943) for a 144-site triangular lattice with  $S = 0.05$  (uniform ground state). The complex argument of  $dA/A$  take only two values:  $\pm\pi/2$  (blue and yellow), indicating that  $dA$  is a (gapped  $U(1)$ ) gauge excitation. Bottom: Infinitesimal flux variation  $dF$  associated to the gauge mode above. For each diamond the magnitude of the flux variation is indicated by the radius of the dot in its center (see color scale for the sign).

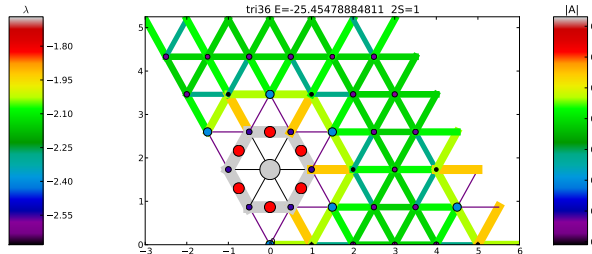


FIG. 10: First excited state on a triangular cluster with 36 sites and  $S = 0.5$ . The bond moduli are invariant by lattice rotations about the site largest chemical potential (grey circle). The flux vanish on all diamonds except for the six diamonds which diagonal bond is marked by a red dot. The later have flux  $\pi$ . Notice the similarity with Fig. 4.

apart in the magnetic phase of the model. Since the system is magnetically ordered, visons are no longer low-energy excitations. Starting from a vison-pair trial state we look for the nearest self-consistent mean field state. A typical result is shown in Fig. 15, where the initial state was chosen to have two localized visons at the same locations as in Fig. 13. At the end of the numerical optimization (stage 2 only), it appears the algorithm has converged to a (unstable) saddle points where some ad-

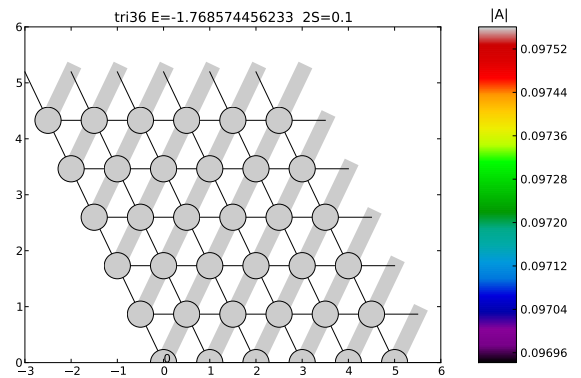


FIG. 11: First excitation on a triangular cluster with 36 sites and  $S = 0.05$ . This state is three-fold degenerate. With the ground state, it forms the four-fold topological degeneracy expected for a  $\mathbb{Z}_2$  liquid on a torus. Notice (scale on the right) that the difference between the largest  $|A_{ij}|$  and the smallest one is only  $\sim 6 \cdot 10^{-4}$  and should vanish in the thermodynamic limit.

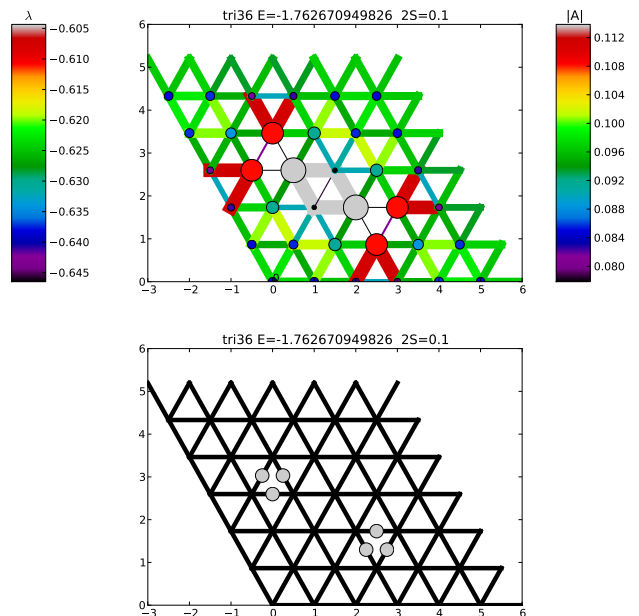


FIG. 12: Top Modulus  $|A|$  and chemical potential for a saddle point with two visons at distance  $d = 5\sqrt{3}/3$ , ( $6 \times 6$  triangular lattice,  $S = 0.1$ ). Bottom: the flux vanishes on all diamonds except those with the diagonal tagged with a grey circle. The visons are localized on the triangles with three such circles.

ditional pairs diamonds with flux  $\pi$  are present. These additional fluxes form an elongated ring enclosing the two initial vison cores. Contrary to the vison-pair states in the liquid phase, the spin-spin correlations are strongly modified all the way inside the ring (bottom panel of 15). Indeed, the three sublattice is destroyed, although the spin spin correlations remain large (black circle radii).

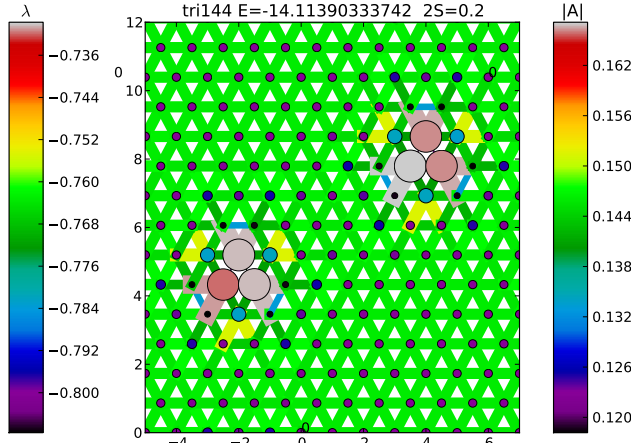


FIG. 13: Modulus  $|A|$  and chemical potential for a saddle point with two visons at distance  $d = 4\sqrt{3}$ , ( $12 \times 12$  triangular lattice,  $S = 0.1$ ). A string of reversed  $A_{ij}$  (not shown) goes from the first vison core to the second.

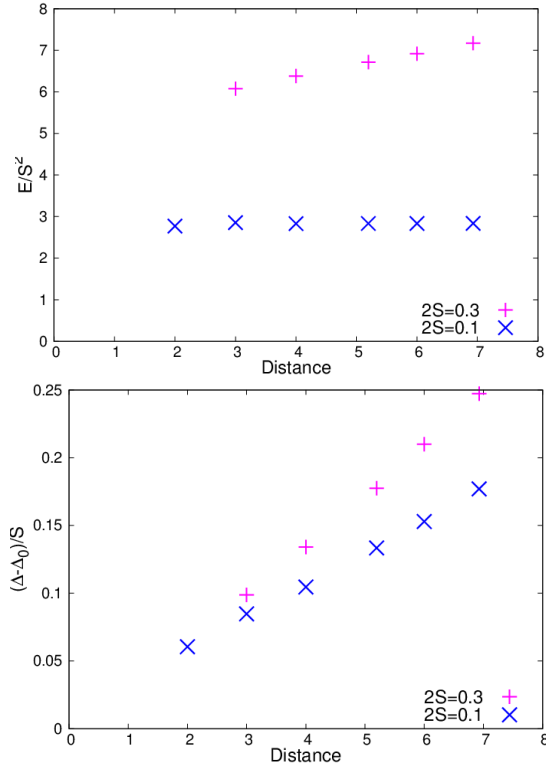


FIG. 14: top: Energy cost of a pair of visons as a function of distance in a 144-site triangular cluster. Bottom: difference between the spinon gap  $\Delta$  in presence of the two visons, and the gap  $\Delta_0$  in the absence of visons. This difference has been scaled by  $S$  to compare  $S = 0.05$  and  $S = 0.15$ . Since  $\Delta > \Delta_0$ , there is some *repulsion* between a spinon and a vison pair.

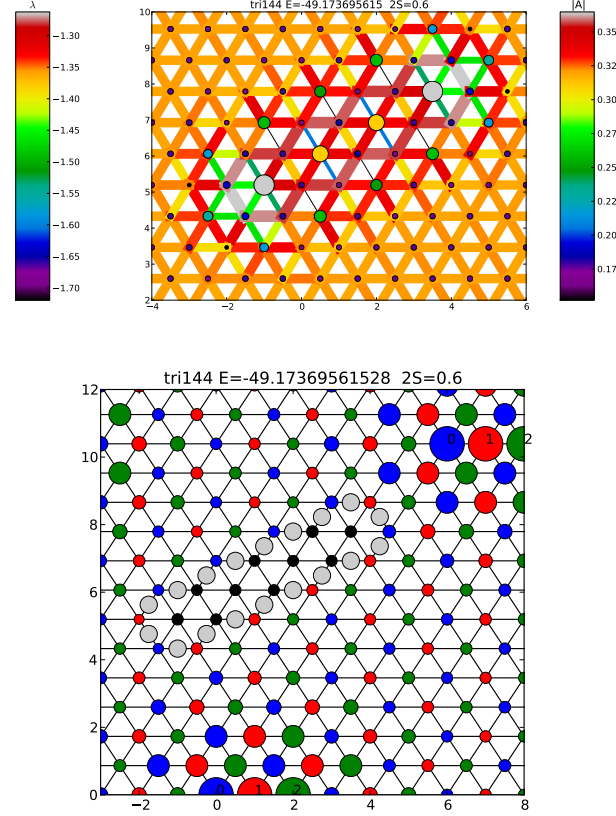


FIG. 15: Highly excited solution on the triangular lattice (144 sites) with  $S = 0.3$  (ordered phase). Top: bond amplitudes. Bottom: Spin-spin correlations and fluxes. If  $\langle S_0 \cdot S_i \rangle$  is positive while  $\langle S_1 \cdot S_i \rangle$  and  $\langle S_2 \cdot S_i \rangle$  are negative, the site  $i$  is said to belong to the “0” sublattice (blue circles). Likewise, the site which are positively correlated with site 1 (resp. 2) are marked in red (resp. green). The other sites are marked in black and the radius of the circle is proportional to the maximum of  $|\langle S_0 \cdot S_i \rangle|$ ,  $|\langle S_1 \cdot S_i \rangle|$  and  $|\langle S_2 \cdot S_i \rangle|$ . The diamonds have vanishing flux except for those marked by a grey circle, which have a flux  $\pi$  (see text).

This state appears to be similar to a classical vortex/anti-vortex pair.

### C. kagome lattice

This section presents some preliminary results for the kagome lattice antiferromagnet.

We explored the low-energy saddle points for kagome clusters with 36 and 48 sites, with boson densities  $S = 0.5$  and  $S = 0.1$ . In all these cases, the ground state is found to have the same *modulated* spatial structure. As show in Fig. 16, the solution spontaneously breaks some lattice symmetries, with two different values for the bond amplitudes. This state has some magnetic long-range order for  $S = 0.5$  (in the thermodynamic limit) and the three-sublattice structure is shown in Fig. 16. It appears that

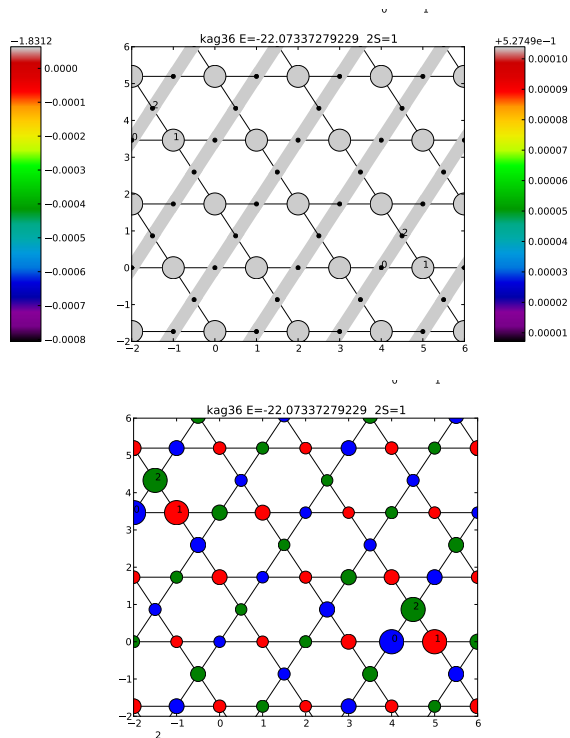


FIG. 16: Lowest-energy mean field solution on a kagome cluster with 36 sites and  $S = 0.5$ . Top panel: the modulus of the bond parameter and the value of the chemical potentials are indicated. Bottom: three-sublattice structure of the spin-spin correlation functions. This state has correlations which are neither of the  $q = 0$  nor  $\sqrt{3} \times \sqrt{3}$ -type.

this state is not of the  $q = 0$  type, nor  $\sqrt{3} \times \sqrt{3}$ . Instead, the three-sublattice structure has a preferred lattice direction (that of lines with green and blue sites only in Fig. 16) and this leads to an enhancement of  $|A_{ij}|$  for the bonds aligned with that direction. The 120 degrees sublattice structure also implies values 0 or  $\pi$  for all the fluxes. In the present case the flux vanishes on all the hexagons, stars, and length-8 rhombi. It however has flux  $\pi$  on some other loops of length 8 and 10. Note that, as remarked by Tchernyshyov *al.*<sup>29</sup>, it is not possible to construct a state with zero flux on all loops on the kagome lattice.

Our preliminary calculations on a 108 site cluster shows that the striped phase is no longer the ground state on larger systems. Due to the complex energy landscape (high density of low energy saddle point) and due to the large system size, it is numerically demanding to sample the solutions starting from random initial conditions on the 108 site kagome cluster (as we did for the 36 and 48 sites clusters). So far we resorted to look at some known solutions and perturbation around them.

On the 108 site cluster, the  $\sqrt{3} \times \sqrt{3}$  turns out to be slightly lower than the “stripe” state (Tab. V). We conclude that with 36 and 48 sites, the striped state is stabilized through resonance loops (of length 6 or 8) which

wind around the periodic boundary conditions. Still, the uniform  $\sqrt{3} \times \sqrt{3}$  state is not ground state either on the 108 site cluster since it possesses some negative Hessian eigenvalue. Work is in progress to find the absolute energy minimum on this cluster.

### 1. Excited saddle points and Hessian eigenvalues

A striking fact concerning the mean field states on the kagome lattice is the high density of saddle points and local minima, as can be seen in Tab. V. The energy differences and the bond and site modulations are very small. For this reason, a high accuracy is needed to resolve the different saddle points and their (tiny) spatial modulations. It is also interesting to note that the lowest Hessian eigenvalues are two orders of magnitude smaller than in the triangular lattice. Although this should be related to the large degeneracy in the classical limit (large  $S$ ), we note that the lowest Hessian eigenvalues are also surprisingly very small in the spin-gapped phase at small  $S$  (data not shown). This very weak energy curvature implies that, unless  $N$  is very large, the bond fluctuations will be very important at finite  $N$ .

Sachdev<sup>9</sup> considered the first quantum corrections to the energy of various coplanar and non-coplanar spin configurations. He found that coplanar states have a lower energy, and the degeneracy among coplanar states is itself lifted (by a small amount) in favor of the  $\sqrt{3} \times \sqrt{3}$  structure. His calculation assumed some homogeneous  $|A_{ij}|$  and  $\lambda_i$ , although the self consistent states associated to some generic classical planar state will break the equivalence between all the bonds and all the sites. Our calculations do take into account the nonequivalence between sites and bonds and thus gives the true saddle point energies. The saddle points we obtain are clearly related to classical planar states, and the underlying planar order is easily revealed by looking at the spin-spin correlations.

As an example, Fig. 17 shows the bond modulations and three-sublattice structure of the first excited saddle point (36 sites,  $S = 0.5$ ). In this particular example, the hexagons with only two colors correspond to (slightly) weaker  $|A_{ij}|$ , and thus higher energy. This is somewhat counter intuitive since one could have expected these spins to resonate between configurations and thus to lower the energy on these bonds. Also, the state with  $\sqrt{3} \times \sqrt{3}$  order is also among the low-energy local energy minima on the 36 site cluster (line *a* in Tab. V). The state with  $q = 0$  order is significantly higher and thus not among the first saddle points.

Finally we note that the numerous complex (chiral) states we obtain must correspond to some non-planar spin structures. Among the non-planar states, the cuboc1 (second line in Tab. VI) is of particular interest. This chiral state (complex  $A_{ij}$ ) with a twelve sublattice magnetic structure<sup>35</sup> has recently been shown by Messio *et al.*<sup>16</sup> to be energetically lower than the  $\sqrt{3} \times \sqrt{3}$  state if both  $A_{ij}$  and  $B_{ij}$  parameters are included in the



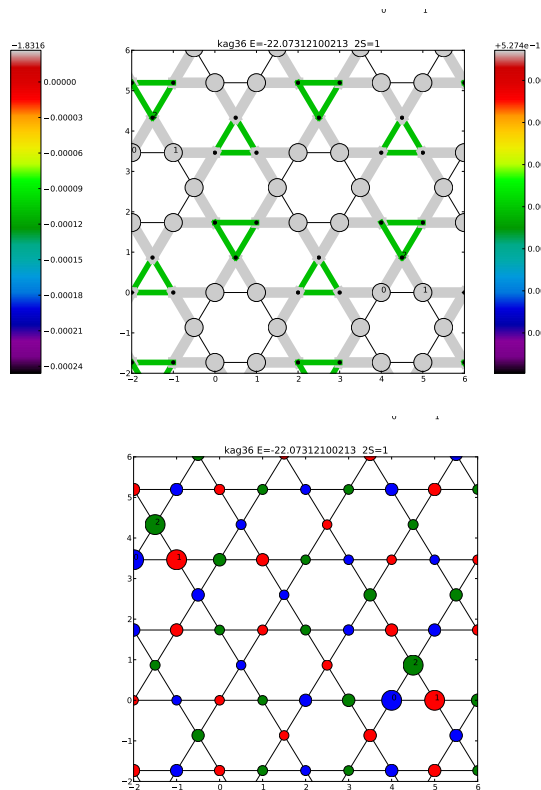


FIG. 17: Excited solution on a kagome cluster with 36 sites. Top: bond moduli (right scale) and chemical potentials (right scale). Bottom: Three-sublattice structure. The radius of each circle is proportional to  $|\langle \vec{S}_a \cdot \vec{S}_i \rangle|$  with  $a = 0, 1$  or  $2$  depending on the sublattice (color).

SBMFT. The present Hessian calculation shows that it is a stable local minimum on the 108-site cluster, at least for the spin values we looked at (from  $S = 0.05$  to  $0.6$ ), both in the spin-gapped (chiral spin liquid) and magnetically ordered phases. As for all the low-energy saddle points we found on the kagome lattice, the lowest Hessian eigenvalue is very small ( $0.0012591460$  for  $S = 0.5$  and  $1.6079020310 \times 10^{-5}$  for  $S = 0.05$ ), indicating a very small energy scale and important finite- $N$  corrections.

## V. CONCLUSION

We have developed a numerical method to explore in a systematic way the low energy SBMFT solutions on finite clusters up to one hundred sites. This gives us

access to an energy landscape which contains some informations about excitations such as gauge modes (“photon” in the Coulomb phase of the square lattice) and topological excitations such as visons ( $\mathbb{Z}_2$  liquid on the triangular lattice). On the kagome lattice this approach reveals a complex landscape with tiny energy scales, and some unexpected magnetic ordering on small clusters.

Work is in progress toward a better understanding of

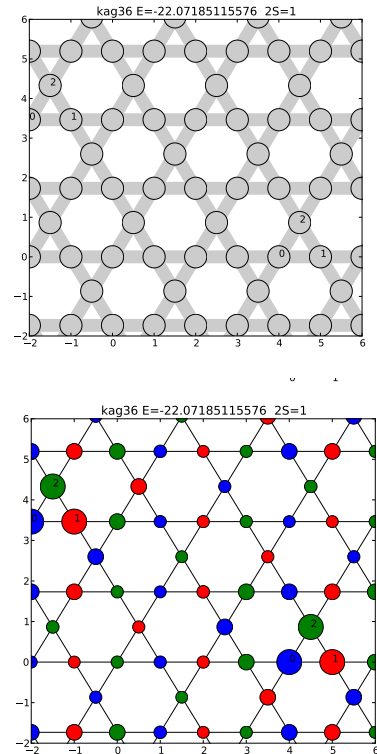


FIG. 18: Uniform mean field solution on a kagome cluster with 36 sites and  $S = 0.5$ . Top panel: the modulus of the bond parameter and the value of the chemical potentials are indicated. Bottom: three-sublattice structure ( $\sqrt{3} \times \sqrt{3}$ ) of the spin-spin correlation functions.

the large- $N$  kagome physics as well as quantitative evaluation of the  $1/N$  effects in the spin-gapped phase as well as in the ordered phase.

*Acknowledgments* — I wish to thank Laura Messio, Claire Lhuillier, Vincent Pasquier and Roderich Moessner for useful discussions. Part of the calculations were performed on the **titane** computer at the *Centre de Calcul Recherche et Technologie* of the CEA.

<sup>1</sup> L. Balents, *Nature* **464**, 199 (2010).

<sup>2</sup> I. Affleck, *Phys. Rev. Lett.* **54**, 966 (1985)

<sup>3</sup> N. Read and S. Sachdev, *Phys. Rev. Lett.* **66**, 1773 (1991).

<sup>4</sup> D. Rokhsar, *Phys. Rev. B* **42**, 2526 (1990).

<sup>5</sup> A. E. Trumper, L. O. Manuel, C. J. Gazza, and H. A. Ceccatto, *Phys. Rev. Lett.* **78**, 2216 (1997).

<sup>6</sup> N. Read and S. Sachdev, *Phys. Rev. Lett.* **62**, 1694 (1989).

<sup>7</sup> D. Arovas and A. Auerbach, *Phys. Rev. B* **38**, 316 (1988).

$E$	$\Delta$	$H$	d	$N_\lambda$	$\min_\lambda$	$\max_\lambda$	$N_{ A }$	$\min_{ A }$	$\min_{ A }$	
-22.07337279228	0.12515086051	0.0089249516	3	2	-1.83200573771	-1.83113623765	2	0.52749717421	0.52759396847	R
-22.07312100213	0.12543211456	0.0107154849	4	2	-1.83184586807	-1.83157327614	3	0.52745562491	0.52757074339	R
-22.07185115575 <sup>a</sup>	0.12538354127	0.0089311159	1	1	-1.83167736298	-1.83167736298	1	0.52751942536	0.52751942536	R
-22.06817893625	0.12503501657	-0.0112835686	12	5	-1.83240200322	-1.83097449336	7	0.52698803771	0.52765000379	C
-22.06448876483	0.12492274319	-0.0129952310	12	5	-1.83195203206	-1.83036801265	7	0.52723842679	0.52764855532	R
-22.06414194485	0.12496054795	-0.0027056846	72	21	-1.83279521914	-1.83033540812	36	0.52699979179	0.52787033175	C
-22.06206958387	0.12456300988	-0.0153407835	36	11	-1.83291554283	-1.83063480061	18	0.52715425178	0.52763583076	C
-22.06206940890	0.12456241439	-0.0161155470	18	7	-1.83291658623	-1.83070454575	9	0.52719208674	0.52761532928	R
-22.06186658368	0.12488134890	-0.0031621455	36	12	-1.83448571023	-1.83020247256	18	0.52671374288	0.52785086628	C
-22.06162809838	0.12509708999	0.0001939410	72	19	-1.83245235549	-1.82999027588	38	0.52684964508	0.52838268073	C
-22.06162809838	0.12509708999	0.0001939410	72	19	-1.83245235550	-1.82999027588	38	0.52684964508	0.52838268073	C
-22.06132041734	0.12484489112	-0.0102590748	72	21	-1.83551900593	-1.82898234568	36	0.52632645045	0.52871495375	C

TABLE V: Some SBMFT saddle points for a kagome lattice cluster with 36 sites with  $2S = \kappa = 1$ . Notice also the high density of local minima and saddle points. The ground state ( $E = -22.07337279228$ ) corresponds to Fig. 16. Line <sup>a</sup> ( $E = -22.071851155756$ ): uniform solution shown in Fig. 18. It has zero flux on the hexagons and 8-sites rhombi, and  $\sqrt{3} \times \sqrt{3}$  magnetic order.

$E$	$\Delta$	$H$	d	$N_\lambda$	$\min_\lambda$	$\max_\lambda$	$N_{ A }$	$\min_{ A }$	$\min_{ A }$	
0-hex,0-rhom ( $\sqrt{3} \times \sqrt{3}$ ) -65.19595579390 <sup>a</sup>	0.05035952577	-0.0006338181	1	1	-1.82031174634	-1.82031174634	1	0.52527760692	0.52527760692	R
cuboc1 -65.18108305169	0.05032119115	0.0012591460	1	1	-1.82017336946	-1.82017336946	1	0.52524483499	0.52524483499	C
$\pi$ -hex,0-rhom ( $q = 0$ ) -64.96199404178	0.04930776212	-0.0660018532	1	1	-1.81849693150	-1.81849693150	1	0.52476183760	0.52476183760	R
Stripe state -63.10095974957	0.07743958702	-31.5397600273	3	2	-1.78528910388	-1.72569936368	2	0.51856978854	0.52475885718	R

TABLE VI: Four saddle points for a kagome lattice cluster with 108 sites with  $2S = \kappa = 1$ . <sup>a</sup> is uniform and corresponds to the 0hex-0rhom<sup>14</sup> state ( $Q_1 = -Q_2$  in Sachdev's<sup>9</sup> terminology) and  $\sqrt{3} \times \sqrt{3}$  magnetic r. It possesses an instability mode (negative Hessian value), which is a pure *gauge* excitation (variation of the phases of  $A_{ij}$  only, no variation of the moduli). This mode is 12-fold degenerate. The cuboc1 was discussed using SBMFT by Messio *et al.*<sup>16</sup>, it has a twelve-sublattice non-planar magnetic structure for large enough  $S$ , and it describes a gapped chiral spin liquid at small  $S$ . The Hessian is gapped, and the associated mode is a 12-fold degenerate gauge mode for  $S = 0.5$ . The stripe state (which is the ground state on 36 and 48-sites clusters) is no longer the lowest energy solution for this 108-site cluster.

- <sup>8</sup> F. Mila, D. Poilblanc and C. Bruder, Phys. Rev. B **43**, 7891 (1991).
- <sup>9</sup> S. Sachdev, Phys. Rev. B **45**, 12377 (1992).
- <sup>10</sup> C. J. Gazza and H. A. Ceccatto, J. Phys.: Condens. Matter **5**, L135 (1993).
- <sup>11</sup> C. H. Chung, J. B. Marston and R.H. McKenzie, J. Phys.: Condens. Matter **13**, 5159 (2001).
- <sup>12</sup> A. Mattsson, P. Fröjdh and T. Einarsson, Phys. Rev. B **49**, 3997 (1994).
- <sup>13</sup> F. Wang, Phys. Rev. B **82**, 024419 (2010).
- <sup>14</sup> F. Wang and A. Vishwanath, Phys. Rev. B **74**, 174423 (2006).
- <sup>15</sup> Tiamhock Tay and O. I. Motrunich, Phys. Rev. B **84**, 193102 (2011).
- <sup>16</sup> L. Messio, B. Bernu, C. Lhuillier, Phys. Rev. Lett. **108**, 207204 (2012).
- <sup>17</sup> B. Fåk *et al.*, preprint [arXiv:1203.6107](https://arxiv.org/abs/1203.6107).
- <sup>18</sup> M. Albrecht and F. Mila, Europhys. Lett. **34**, 145 (1996).
- <sup>19</sup> C. H. Chung, J. B. Marston and S. Sachdev, Phys. Rev. B **64**, 134407 (2001).
- <sup>20</sup> M. Albrecht and F. Mila, Phys. Rev. B **53**, R2945 (1996).
- <sup>21</sup> M. Hermele, V. Gurarie, and A. M. Rey, Phys. Rev. Lett. **103**, 135301 (2009); M. Hermele and V. Gurarie Phys. Rev. B **84**, 174441 (2011).
- <sup>22</sup> A. Auerbach, *Interacting electrons and Quantum Magnetism*, Springer-Verlag, 1994.
- <sup>23</sup> G. Misguich, Lectures notes of the Les Houches summer school on "Exact Methods in Low-dimensional Statistical Physics and Quantum Computing", July 2008, preprint [arXiv:0809.2257](https://arxiv.org/abs/0809.2257)
- <sup>24</sup> H. A. Ceccatto, C. J. Gazza, and A. E. Trumper, Phys. Rev. B **47**, 12329 (1993)
- <sup>25</sup> R. Flint and P. Coleman; Phys. Rev. B **79**, 014424 (2009).
- <sup>26</sup> This mean field Hamiltonian is the same as that obtained in the  $N \rightarrow \infty$  limit of the  $Sp(N)$  generalization of the Heisenberg model.<sup>3</sup> Another possibility is to keep *both* the ferro- and anti-ferro mean field parameters.<sup>24</sup>
- <sup>27</sup> J. H. P. Colpa, Physica A **93**, 327 (1978).
- <sup>28</sup> From Eq. 12 we have  $\partial E / \partial \lambda = \kappa - \langle \hat{n}_i \rangle$  and  $\partial^2 E / \partial \lambda^2 = -\partial \langle \hat{n}_i \rangle / \partial \lambda$ . Using first order perturbation theory the last expression can be shown to be negative.
- <sup>29</sup> O. Tchernyshyov, R. Moessner and S. L. Sondhi, Europhys. Lett. **73**, 278 (2006).
- <sup>30</sup> M. I. A. Lourakis, levmar: Levenberg-Marquardt nonlinear least squares algorithms in C/C++, <http://www.ics.forth.gr/~lourakis/levmar/>.
- <sup>31</sup> L. Messio, Ph.D thesis, Université P. et M. Curie, (2010).
- <sup>32</sup> X.-G. Wen, Phys. Rev. B **65**, 165113 (2002).
- <sup>33</sup> N. Read and B. Chakraborty, Phys. Rev. B **40**, 7133 (1989).
- <sup>34</sup> Y. Huh, M. Punk and S. Sachdev, Phys. Rev. B **84**, 094419 (2011).
- <sup>35</sup> O. Janson, J. Richter, and H. Rosner, J. Phys.: Conf. Ser. **145**, 012008 (2009).